Bcc crystal-fluid interfacial free energy in Yukawa systems

V. Heinonen, A. Mijailović, C. V. Achim, T. Ala-Nissila, R. E. Rozas et al.

Citation: J. Chem. Phys. **138**, 044705 (2013); doi: 10.1063/1.4775744
View online: http://dx.doi.org/10.1063/1.4775744
View Table of Contents: http://jcp.aip.org/resource/1/JCPSA6/v138/i4
Published by the American Institute of Physics.

Bcc crystal-fluid interfacial free energy in Yukawa systems

V. Heinonen,[1] A. Mijailović,[2] C. V. Achim,[1,2] T. Ala-Nissila,[1,3] R. E. Rozas,[2] J. Horbach,[2] and H. Löwen[2]

[1]*COMP Centre of Excellence, Department of Applied Physics, Aalto University, School of Science, P.O.Box 11100, FI-00076 Aalto, Finland*

[2]*Institut für Theoretische Physik II: Weiche Materie, Heinrich-Heine-Universität Düsseldorf, Universitätsstraße 1, D-40225 Düsseldorf, Germany*

[3]*Department of Physics, Brown University, Providence, Rhode Island 02912-1843, USA*

(Received 1 August 2012; accepted 27 December 2012; published online 23 January 2013)

We determine the orientation-resolved interfacial free energy between a body-centered-cubic (bcc) crystal and the coexisting fluid for a many-particle system interacting via a Yukawa pair potential. For two different screening strengths, we compare results from molecular dynamics computer simulations, density functional theory, and a phase-field-crystal approach. Simulations predict an almost orientationally isotropic interfacial free energy of $0.12k_BT/a^2$ (with k_BT denoting the thermal energy and a the mean interparticle spacing), which is independent of the screening strength. This value is in reasonable agreement with our Ramakrishnan-Yussouff density functional calculations, while a high-order fitted phase-field-crystal approach gives about 2−3 times higher interfacial free energies for the Yukawa system. Both field theory approaches also give a considerable anisotropy of the interfacial free energy. Our result implies that, in the Yukawa system, bcc crystal-fluid free energies are a factor of about 3 smaller than face-centered-cubic crystal-fluid free energies. © *2013 American Institute of Physics*. [http://dx.doi.org/10.1063/1.4775744]

I. INTRODUCTION

Both crystallization and melting phenomena involve solid-liquid interfaces that separate the ordered from the disordered phase. It is important to understand structural and dynamical properties of crystal-fluid interfaces on a microscopic scale in order to control and steer the nucleation and subsequent growth of the crystal. One of the key static properties of the crystal-fluid interface at coexistence is its interfacial free energy,[1] which measures the free energy penalty per area paid for the interface creation. Unlike for liquid-gas or fluid-fluid interfaces, this free energy depends on the orientation of the interface relative to the crystal axes.

It is challenging to calculate and predict actual values for the crystal-fluid interfacial free energy for a given interparticle interaction, typically described by a pairwise potential $V(r)$ with r denoting the interparticle separation. Recently, simulation schemes have been developed to access the interfacial free energy by studying the capillary wave fluctuations.[2–8] Even more challenging is a molecular theory predicting interfacial free energies. A necessary requirement to such theory is that it has to describe the crystal and the fluid phase in a unifying way. Classical density functional theory (DFT) of freezing[9–12] is one of the few (if not the only) approaches, which fulfills this requirement. There have been many approximation schemes and studies for the hard-sphere system including the interfacial free energy of the hard sphere face-centered-cubic (fcc) crystal-fluid interface.[8,13–16] However, beyond hard-sphere perturbation theory,[14,17–20] systems with a softer pair interaction $V(r)$ are much less studied.[21–23] In the latter case, the Ramakrishnan-Yussouff perturbative density functional theory[24] or some mean-field variants[23] can be applied in principle, which yield acceptable results for freezing of Yukawa systems,[23] for more sophisticated functionals (see Ref. 25–27).

DFT has also been shown[28–30] to be an ideal framework to derive more coarse-grained models for crystallization, such as the phase-field-crystal (PFC) model as put forward by Elder and co-workers.[31,32] PFC models typically involve much less numerical effort to access the phase diagram than full DFT calculations. A high-order fitting procedure enables a realistic PFC model, which reproduces the basic features of crystallization and has been shown to give good quantitative results for the interfacial free energy and grain boundary free energies in the case of body-centered-cubic (bcc) iron.[33–35]

In this paper, we address the crystal-fluid interfacial free energies for a Yukawa (i.e., screened Coulomb) system,[23] which is characterized by the pair potential $V(r) = u_0 \exp(-\kappa r)/r$ where u_0 is an interaction amplitude and κ denotes the inverse screening length. The soft Yukawa potential has been used to describe the effective interaction between charged colloids immersed in an electrolyte solution[36–38] or between two dust particles in a plasma.[39–41] Interestingly, depending on the dimensionless parameter κa with $a = \rho^{-1/3}$ denoting the mean interparticle distance at a given number density ρ, the Yukawa system[23] exhibits both stable body-centered-cubic (bcc) crystals at low $\kappa a < 5$ and face-centered-cubic (fcc) crystals at large $\kappa a > 5$.[42–45] Here, we focus on the Yukawa bcc crystal-fluid interface, which has neither been studied before by simulation, nor by density functional theory. We determine its orientation-resolved interfacial free energy. For two different screening strengths κa, we compare results from molecular dynamics (MD) computer simulations, DFT

and a PFC approach. Our simulations predict an orientationally fairly isotropic interfacial free energy of about $0.12k_BT/a^2$ with k_BT denoting the thermal energy, which turns out to be almost independent on the screening strength. Such a value is in reasonable agreement with our Ramakrishnan-Yussouff density functional calculations, while a high-order fitted PFC approach predicts interfacial energies, which are about 2−3 times higher. In addition, both DFT and PFC predict considerable interfacial anisotropy in contrast to the MD results.

Our result implies that in Yukawa systems,[23] bcc crystal-fluid free energies are significantly smaller than face-centered-cubic (fcc) crystal-fluid free energies, which vary typically between $0.4k_BT/a^2$ for Yukawa systems[46] and $0.65k_BT/a^2$ for hard spheres.[8] This drastic reduction of the interfacial free energy agrees with the Spaepen-Meyer theory,[47,48] and is consistent with the Alexander-McTague theory,[49] which predicts that the bcc-crystal is structurally closer to the liquid than the fcc-crystal.

The paper is organized as follows: in Sec. II, we briefly describe our simulation method while Sec. III contains the density functional calculations. Section IV is devoted to the phase-field crystal model. Our results are presented and discussed in Sec. V, and our summary and conclusions in Sec. VI.

II. COMPUTER SIMULATIONS OF INTERFACE FREE ENERGY

We determine "reference values" for the anisotropic interfacial free energies of bcc crystal-fluid interfaces by molecular dynamics (MD) computer simulations. To this end, Newton's equations of motion are solved describing the interactions between the particles by a Yukawa pair potential that is cut off and shifted to zero at the distance $r = r_{\rm cut}$ between a pair of particles. The potential is given by

$$V(r) = \begin{cases} [u(r) - u(r_{\rm cut})]\, S_{\rm cut}(r), & \text{for } r < r_{\rm cut}, \\ 0, & \text{for } r \geq r_{\rm cut}, \end{cases} \tag{1}$$

where $u(r)$ and $S_{\rm cut}(r)$ are defined by

$$u(r) = \frac{u_0}{r}\exp(-\kappa r) = \frac{\varepsilon}{\kappa r}\exp(-\kappa r), \tag{2}$$

$$S_{\rm cut}(r) = \frac{(r - r_{\rm cut})^4}{h + (r - r_{\rm cut})^4}. \tag{3}$$

In Eq. (2), $\varepsilon = u_0\kappa$ sets the energy scale of the potential. The function $S_{\rm cut}(r)$ ensures that both energies and forces are continuous at the cut-off distance $r_{\rm cut}$. We have found that the choice $h = 0.01$ in $S_{\rm cut}(r)$ does not significantly affect the shape of the Yukawa potential (as well as the forces) while it leads to an efficient smoothing of $V(r)$ around $r = r_{\rm cut}$. The cut-off is set to $r_{\rm cut} = 9/\kappa$.

In the following, reduced variables are labeled by primes. Reduced distances, energies, pressures and temperatures are given by $r' = r\kappa$, $E' = E/\varepsilon$, $P' = P\kappa^3/\varepsilon$, and $T' = k_BT/\varepsilon$, respectively. Time is measured in units of the characteristic time scale $\tau = \kappa\sqrt{\varepsilon/m}$ (m is the mass of a particle) and thus $t' = t/\tau$. At a given reduced temperature T', the reduced parameter $a' = \kappa a$ (with $a = \rho_{\rm s}^{-1/3}$ and $\rho_{\rm s}$ the density of the solid phase) controls the phase behavior of the Yukawa model. In this work, we consider $a' = 2.5$ and $a' = 4.0$; in both cases, the system exhibits a transition from a fluid to a crystal bcc phase.

The methodology for the calculation of the interfacial free energy is similar to that used for other systems such as hard spheres[6,8] or Ni.[7] First, the melting temperature $T_{\rm m}$ is determined by analyzing the growth of inhomogeneous solid-fluid systems at various undercoolings. Then, systems with solid-fluid interfaces at $T_{\rm m}$ are prepared to analyze the long-wavelength capillary wave fluctuations along the interface. From this analysis, the interfacial stiffness $\bar{\gamma}_{\alpha\beta}(\hat{n})$ for the crystal orientations (100), (110), and (111), corresponding to different normal unit vectors $\hat{n}$ relative to the crystal lattice, are determined. The interfacial stiffness $\bar{\gamma}_{\alpha\beta}(\hat{n})$ is related to the anisotropic interfacial free energy $\gamma(\hat{n})$ by

$$\bar{\gamma}_{\alpha\beta}(\hat{n}) = \gamma(\hat{n}) + \frac{\partial^2\gamma(\hat{n})}{\partial\hat{n}_\alpha\partial\hat{n}_\beta}, \tag{4}$$

where the unit vectors $\hat{n}_\alpha$ and $\hat{n}_\beta$ indicate two directions in the interface plane that are orthogonal to $\hat{n}$. To obtain the interfacial free energy $\gamma(\hat{n})$ from the interfacial stiffness $\bar{\gamma}_{\alpha\beta}(\hat{n})$, the latter quantity is parameterized in terms of a cubic harmonic expansion, which then allows to estimate also $\gamma(\hat{n})$ for different orientations (see below).

The equations of motion were integrated by the velocity form of the Verlet algorithm using a time step $\Delta t' = 1.0$. The systems were coupled to a thermostat and a barostat in order to perform the simulations at constant temperature T and constant pressure P, respectively. Temperature was kept constant by reassigning every 200 steps new velocities to each particles according to a Maxwell-Boltzmann distribution. For the simulation at constant pressure P, an algorithm proposed by Andersen[50] was used.

The melting temperature $T'_{\rm m}$ was determined from the simulation of inhomogeneous systems where the crystalline phase is surrounded by the liquid phase and separated from it by two planar interfaces (note that two interfaces occur due to periodic boundary conditions). Depending on temperature, the crystal either grows or melts, which is associated with a movement of the interface toward the liquid or the crystal, respectively. The melting temperature $T'_{\rm m}$ is estimated from the temperature dependence of the interface velocity as the point where the interface velocity is zero.[5,7]

To prepare inhomogeneous systems, first, a bulk bcc crystal were placed into an elongated simulation box of size $L'_x \times L'_y \times L'_z$ with $L = L'_x = L'_y = \frac{1}{5}L'_z$ applying periodic boundary conditions in all three dimensions. This system was equilibrated for a given value of a' at a temperature at which the bcc phase is the thermodynamically stable phase. From this simulation, the average pressure P was computed, followed by a simulation where the pressure is kept constant at the latter value. Then, along the z direction two regions were defined in this system: a crystalline region of length $2L$ and a liquid region in the remaining part of the system (with the crystal being in (100) orientation with respect to the liquid). The liquid zone was melted by increasing the temperature well above the melting temperature (which we roughly knew from simulations where we melted the bulk crystalline

phase) while the particles in the crystalline zone were kept at fixed positions. This simulation was done in the NP_zAT ensemble, i.e., at constant area $A = L'_x \times L'_y$ and constant pressure in z direction, P_z. In the next step, the liquid was cooled down to the initial temperature and now simulations in the NP_zAT ensemble were performed where the crystalline particles were again free to move. After a short relaxation of the interface, the growth of the stable phase was analyzed, thus extracting the interface velocity at the considered temperature T. The same procedure was done at eight different temperatures thus allowing for an accurate extrapolation to the temperature where the interface velocity vanishes. Note that at each temperature eight independent simulations were performed.

We found $T'_m = 0.00202$ for $a' = 2.5$ and $T'_m = 0.000586$ for $a' = 4.0$. Having determined the melting temperature, inhomogeneous solid-fluid systems at T'_m were placed in simulation boxes of size $L'_x \times L'_y \times L'_z$ applying periodic boundary conditions in all three dimensions. As before, the box lengths L'_x, L'_y, L'_z were chosen such that L'_z is about five times larger than L'_x and L'_y. In z direction, the bcc crystal had an extension of about $\frac{2}{5}L'_z$ and was separated from the fluid by two planar interfaces.

The starting point for the preparation of the inhomogeneous solid-fluid systems was a pure bcc crystal in a simulation box with the aforementioned geometry. The bcc crystal was equilibrated in the NPT ensemble at $T = T_m$. Then, particles in the middle of the box (with an extension of $\frac{2}{5}L'_z$ in z direction) were fixed and the rest of the system was melted at a temperature well above T_m. In the latter step, the simulation was done in the NP_zAT ensemble. Setting temperature back to T_m and allowing all particles to move, the simulations were continued in the NP_zAT ensemble. The system was equilibrated for 2×10^5 time steps, followed by a production run over 10^5 steps where every 10^3 time steps a configuration for the capillary wave analysis was stored. Note that we monitored the non-diagonal elements of the stress tensor during our simulations to check that no stresses were generated in the bulk region of the solid. In fact, we found that the stresses were fluctuating around zero during all the production runs.

For each of the two systems with $a' = 2.5$ and $a' = 4.0$, the three crystal orientations (100), (110), and (111) were considered and 120 independent runs were performed in each case from which about 12 000 configurations were obtained in each case for the capillary wave analysis. The box geometries and the number of particles (around $N = 150\,000$) are listed in Table I.

TABLE I. Box lengths L'_x, L'_y, and L'_z, pressure P' and particle number N used in the MD simulations for $a' = 2.5$ and $a' = 4.0$.

Orientation	a'	P'	L'_x	L'_y	L'_z	N
(100)	2.5	0.0162	82.01	82.01	410.57	175760
(110)	2.5	0.0162	80.3	78.86	401.97	162000
(111)	2.5	0.0162	71.37	69.53	437.61	138240
(100)	4.0	0.000517	126.11	126.11	632.27	175760
(110)	4.0	0.000517	128.41	126.11	643.81	162000
(111)	4.0	0.000517	114.14	111.2	700.87	138240

III. DENSITY FUNCTIONAL THEORY OF FREEZING

Next, we consider the interface free energy in the Yukawa system[23] using field theoretic methods. In the Ramakrishnan-Yussouf density functional theory (DFT) of freezing, the solid state is treated as a perturbation around the liquid state with a freezing density ρ_l. The free energy relative to the liquid free energy is written as

$$\beta\mathcal{F}[\rho(\vec{r})] = \int d\vec{r}[\rho(\vec{r})\log(\rho(\vec{r})/\vec{\rho}_l) - (\rho(\vec{r}) - \rho_l)] - \frac{1}{2}\int d\vec{r}\int d\vec{r}\,'[\rho(\vec{r}) - \rho_l]c(|\vec{r} - \vec{r}\,'|)[\rho(\vec{r}\,') - \rho_l], \tag{5}$$

with $\beta = 1/(k_BT)$ and $c(|\vec{r} - \vec{r}\,'|)$ the two-point direct correlation function calculated at the freezing density. The first part of the free energy in Eq. (5) is the exact free energy of an ideal gas giving rise to entropic effects while the second part accounts for the interactions between particles. Here, the two-point direct correlation function is obtained from a liquid state integral theory, as explained below.

A. Liquid state integral theory

In the liquid state integral theory, the structure of the liquid can be described by using the Ornstein-Zernicke equation, which is an exact relation between the direct correlation function $c(r)$ and the total correlation function $h(r)$,

$$h(r) - c(r) = \rho\int d\vec{r}\,'c(|\vec{r} - \vec{r}\,'|)h(r'). \tag{6}$$

In order to calculate the correlation functions, a second relation known as a closure relation is needed. This relation relates the correlation functions to the pairwise interaction potential as

$$g(r) = \exp[-\beta V(r) + \gamma(r) + b(r)]. \tag{7}$$

Here, $g(r) = h(r) + 1$ is the radial distribution function, $\gamma(r) = h(r) - c(r)$ is the indirect correlation function, and $b(r)$ is a bridge function that contains the contribution of all bridge diagrams. In this work, we use the extended Rogers-Young (ERY) closure relation[51] where the bridge function is defined as

$$b(r) = -\gamma(r) + \log\{1 + \varphi(r) + b_{\mathrm{ERY}}[\varphi(r)]^2\}, \tag{8}$$

where $\varphi(r) = \{\exp[\gamma(r)f(r)] - 1\}/f(r)$ and $f(r) = 1 - \exp(-a_{\mathrm{ERY}}r)$. The parameters a_{ERY} and b_{ERY} are fitted to obtain two equations of thermodynamic consistencies, namely for the normalized isothermal compressibility

$$\chi_c = \chi_V, \tag{9}$$

and another relation relating the pressure to the excess internal energy per particle U,

$$\rho\frac{\partial^2(\rho\beta U)}{\partial\rho^2} = \frac{\partial^2(\beta P)}{\partial\beta\partial\rho}. \tag{10}$$

The compressibility χ_c in Eq. (9) is obtained from the direct correlation function

$$\chi_c = \left[1 - 4\pi\rho \int_0^\infty dr r^2 c(r)\right]^{-1}, \tag{11}$$

while χ_V is taken from the thermodynamic definition

$$\chi_V = \left[\frac{\partial(\beta P)}{\partial \rho}\right]_T^{-1}. \tag{12}$$

Here, the pressure is defined by the virial expansion

$$\beta P = \rho - 4\pi \frac{\rho^2}{6} \int_0^\infty dr r^3 \frac{\partial[\beta V(r)]}{\partial r} g(r). \tag{13}$$

Equation (10) can be written as

$$\rho \frac{\partial^2[\rho\beta U]}{\partial \rho^2} = -\frac{\partial(\rho \hat{c}(0))}{\partial \beta} \tag{14}$$

using Eq. (9). Here, $\hat{c}(0)$ is the zero wave value of the Fourier transform of the direct correlation function $\hat{c}(0) = 4\pi \int_0^\infty dr r^2 c(\vec{r})$, and βU can be obtained using

$$\beta U = 2\pi\rho \int_0^\infty dr r^2 [\beta V(r)] g(r).$$

We tested the ERY method at one point within the Yukawa phase diagram by calculating the correlation functions from independent Monte Carlo (MC) simulations of the corresponding Yukawa particle system. As shown in Fig. 1, the ERY method gives results in excellent agreement with MC.

IV. PHASE-FIELD CRYSTAL MODEL

The phase field crystal (PFC) model is a coarse-grained model in which the free energy is minimized by a periodic density field.[31,32] In this approach, many crystal structure related properties, e.g., multiple grain orientations, dislocations, and anisotropy arise naturally. The PFC Hamiltonian can be derived from the DFT of freezing, as shown in Ref. 28. To this end, we define an adimensional density deviation as

$$n(\vec{r}) = \frac{\rho(\vec{r}) - \rho_l}{\rho_l}. \tag{15}$$

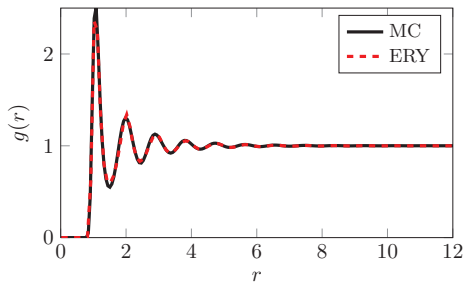

FIG. 1. The radial distribution function as a function of the inter-particle distance r obtained from Monte Carlo simulations and the ERY method ($a' = 3.89$ and $\varepsilon/a' k_B T = 389.47$).

Plugging this into Eq. (5), the free-energy change becomes

$$\beta \mathcal{F}[n(\vec{r})] = \rho_l \int d\vec{r} \{[1 + n(\vec{r})] \log[1 + n(\vec{r})] - n(\vec{r})\} - \frac{\rho_l^2}{2} \int d\vec{r} \int d\vec{r}\,' n(\vec{r}) c(|\vec{r} - \vec{r}\,'|) n(\vec{r}\,'). \tag{16}$$

First, the local part is expanded as a fourth order power series as

$$[1 + n(\vec{r})] \log[1 + n(\vec{r})] - n(\vec{r}) \approx \frac{1}{2} n^2(\vec{r}) - \frac{a_p}{6} n^3(\vec{r}) + \frac{b_p}{12} n^4(\vec{r}). \tag{17}$$

The parameters a_p and b_p are included in the Taylor expansion to allow more freedom in the fitting of the model. A direct Taylor expansion fails due to the fact that n is not really a small parameter. The values for a_p and b_p used here are obtained from a fitting procedure, as described in detail in Ref. 52. A general discussion for the validity of the latter fitting procedure has also recently been given by Oettel *et al.*[53]

Next, the direct correlation function is expanded in k space up to the eighth order:

$$\rho_l \hat{c}_{\mathrm{EOF}}(k) = C(k_m) - E_S \left(\frac{k_m^2 - k^2}{k_m^2}\right)^2 - E_B \left(\frac{k_m^2 - k^2}{k_m^2}\right)^4, \tag{18}$$

where k_m corresponds to the peak of the correlation function. Here, E_S is chosen such that the second derivatives at the peak k_m of the initial correlation function and the fit agree while E_B is chosen in a way to preserve the correct infinite wavelength ($k = 0$) limit.

V. RESULTS

A. Capillary wave analysis from MD simulations

The interfacial stiffness, as defined by Eq. (4), can be obtained from an analysis of the interface height fluctuations $h(\vec{q})$ (with $\vec{q} = (q_x, q_y)$ the two-dimensional wavevector along the lateral extension of the interface). The correlation function of the interface height fluctuations, $\langle h^2(\vec{q})\rangle$, can be related to q-dependent interfacial stiffnesses $\bar{\gamma}_1(q_x)$ and $\bar{\gamma}_2(q_y)$ by[7,8]

$$\bar{\gamma}_1(q_x) q_x^2 + \bar{\gamma}_2(q_y) q_y^2 = \frac{k_B T}{L_x L_y \langle h^2(\vec{q})\rangle}. \tag{19}$$

Whereas, for the (100) and (111) orientations, $\bar{\gamma}_1(q_x)$ is equal to $\bar{\gamma}_2(q_y)$, these coefficients are expected to be different for the (110) orientation. In the latter case, $\bar{\gamma}_1(q_x)$ and $\bar{\gamma}_2(q_y)$ can be extracted from Eq. (19) by setting $q_y = 0$ and $q_x = 0$, respectively. The thermodynamic interfacial stiffnesses are obtained from Eq. (19) in the limit $\vec{q} \to 0$.

In order to determine $h(\vec{q})$, one has to employ a local criterion to distinguish between fluid and crystalline particles. Here, we follow our recent work[7,8] and measure the local order of the particles by the rotational-invariant bond-order

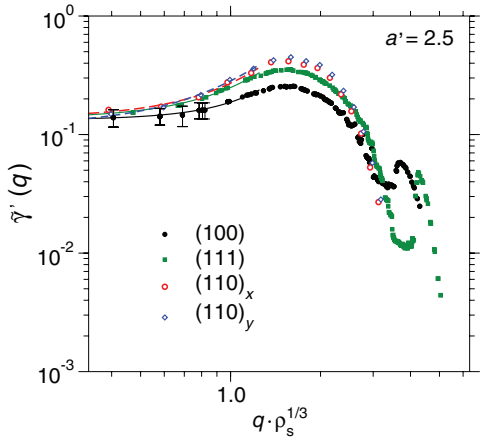

FIG. 2. q-dependent interfacial free energy $\bar{\gamma}'(q) = \bar{\gamma}(q)\rho_s^{-2/3}/(k_B T_m)$ for the (100) and (111) orientations as well as for the two directions of the (110) orientation. Here, the Yukawa system[23] with $a' = 2.5$ is considered. The solid lines are fits from which $\bar{\gamma}$ in the limit $q \to 0$ is extracted (see text). Error bars are shown for the (100) orientation. For the other orientations, similar error bars are obtained (cf. Table II).

parameter $q_6q_6(i)$.[54,55] A particle i is defined as a crystalline one if $q_6q_6(i) > 0.65$. Once crystal and fluid particles are defined, crystalline interface particles are identified as those particles that have more than 5 and less than 12 crystalline neighbors.

The algorithm generates two sets of points $\{(x_i, y_i, z_i)\}$ (one for each interface), which define a surface perpendicular to the z axis. The points on the surfaces are irregularly distributed on the xy plane. The fluctuation of the local interface position is defined as $h(x_i, y_i) = z_i - \langle z_i \rangle$, where i denotes an atom on the surface and the brackets an instantaneous average over these atoms. In order to obtain $\langle h^2(\vec{q}) \rangle$, the points are mapped onto a regular grid on the xy plane using Shepard interpolation,[7] followed by the Fourier transformation of the interpolated heights.

Figure 2 shows the q-dependent interfacial stiffness $\bar{\gamma}(q)$ for the different orientations for the case $a' = 2.5$ (note that the curves for $a' = 4.0$ display a similar behavior and are therefore not shown here). The solid lines are fits with the function $\bar{\gamma}(q) = \bar{\gamma} + c_1 q^2 + c_2 q^4$ (with the three fit parameters $\bar{\gamma}$, c_1, and c_2) from which in the limit $q \to 0$ the stiffness $\bar{\gamma}$ is obtained.[56] The values of $\bar{\gamma}$ for the different orientations, as obtained from the simulation, can be found in Table II. Table III gives the values for the melting temperature and coexistence densities as well as the relative change in density, $\Delta\rho'/\rho_s'$, between the fluid and the crystal phase. The latter values indicate a very small jump in density (i.e., smaller than 1%) for the bcc crystal-to-fluid transition. This small difference in density is associated with a relatively weak anisotropy of the interfacial stiffness (Table II).

TABLE II. Dimensionless values for the stiffnesses ($\tilde{\gamma}\rho_s^{-2/3}/k_B T_m$) from MD simulations.

a'	$\tilde{\gamma}_{100}$	$\tilde{\gamma}_{111}$	$\tilde{\gamma}_{110x}$	$\tilde{\gamma}_{110y}$
2.5	0.132(21)	0.136(15)	0.138(34)	0.120(31)
4.0	0.134(18)	0.137(12)	0.137(25)	0.112(21)

TABLE III. Melting temperature T_m', coexistence densities for the fluid, ρ_l', and the crystal, ρ_s', and $\Delta\rho'/\rho_s' = (\rho_s' - \rho_l')/\rho_s'$, as obtained from the MD simulation (the densities ρ_l' and ρ_s' are given in units of ρ_s/κ^3).

a'	T_m'	ρ_l'	ρ_s'	$\Delta\rho'/\rho_s'$
2.5	0.00202(2)	0.063590(3)	0.063730(3)	0.00211
4.0	0.000586(8)	0.01551(2)	0.01559(2)	0.00553

The interfacial free energy γ can be expanded in terms of cubic harmonics as[57]

$$\frac{\gamma(\hat{n})}{\gamma_0} = 1 + \epsilon_1\left(Q - \frac{3}{5}\right) + \epsilon_2\left(3Q + 66S - \frac{17}{9}\right) + \epsilon_3\left(5Q^2 - 16S - \frac{94}{13}Q + \frac{33}{13}\right), \quad (20)$$

with $Q = n_1^4 + n_2^4 + n_3^4$ and $S = n_1^2 n_2^2 n_3^2$. The components (n_1, n_2, n_3) of the vector normal to the interface $\hat{n}$ are given by $n_i = (\cos\theta\hat{u} + \sin\theta\hat{x}) \cdot \hat{x}_i$ with $\hat{u}$ the crystal orientation and $\hat{x}$ a vector tangential to the interface. The stiffnesses can be parameterized in terms of the parameters γ_0 and ϵ_i by expressing the stiffnesses as $\bar{\gamma} = \gamma + d^2\gamma/d\theta^2$ and evaluating this expression at $\theta = 0$. As a result, four independent equations are obtained

$$\tilde{\gamma}_{100}t + \frac{18}{5}\epsilon_1 + \frac{80}{7}\epsilon_2 + \frac{140}{13}\epsilon_3 = 1, \quad (21)$$

$$\tilde{\gamma}^a_{110}t - \frac{39}{10}\epsilon_1 - \frac{155}{14}\epsilon_2 + \frac{35}{4}\epsilon_3 = 1, \quad (22)$$

$$\tilde{\gamma}^b_{110}t + \frac{21}{10}\epsilon_1 - \frac{365}{14}\epsilon_2 + \frac{175}{52}\epsilon_3 = 1, \quad (23)$$

$$\tilde{\gamma}_{111}t - \frac{12}{5}\epsilon_1 + \frac{1280}{63}\epsilon_2 + \frac{1120}{351}\epsilon_3 = 1 \quad (24)$$

with $t = 1/\gamma_0$. Here, $\tilde{\gamma}^a_{110}$ and $\tilde{\gamma}^b_{110}$ denote the values of the stiffness for the (110) orientation in the tangential directions $[0\bar{1}0]$ and [001], respectively. The parameters γ_0, ϵ_1, ϵ_2, and ϵ_3 that result from fits with Eqs. (21)–(24) are listed in Table IV. From these parameters, the interfacial free energies γ can be estimated using the expansion (20).

TABLE IV. Parameters of the cubic harmonic expansion (see text for details).

a'	γ_0	ϵ_1	ϵ_2	ϵ_3
2.5	0.125(20)	0.0132(2)	−0.00155(3)	−0.00816(23)
4.0	0.120(14)	0.0150(1)	−0.00308(5)	−0.0128(4)

TABLE V. Dimensionless values for the interfacial energies ($\gamma\rho^{-2/3}/k_BT_m$) from MD simulations.

a'	γ_{100}	γ_{110}	γ_{111}
2.5	0.125(20)	0.125(20)	0.124(20)
4.0	0.120(14)	0.120(14)	0.119(15)

The resulting values of γ for different orientations are summarized in Table V. Our main result is that within the error bars the orientational anisotropy of γ appears to be very weak. Moreover, the interfacial free energy γ depends only weakly on the screening parameter a'.

B. Field theoretical approaches

The calculations using both the DFT and PFC models are done by setting up an anisotropic rectangular system box of half bcc crystal, half liquid applying periodic boundary conditions in all three spatial directions. The coexistence densities of the liquid, ρ_l', and the solid, ρ_s', are calculated for reference bulk systems using the common tangent construction. The densities ρ_l' and ρ_s' as well as the melting temperature T_m' from the DFT and PFC calculations are displayed in Table VI. They show good agreement with the simulation data (see Table III).

The equilibrium density profiles are obtained by the minimization of the free energy functionals given by Eq. (5) for the DFT and Eqs. (16)−(18) for the PFC. The minimization was performed by relaxing the generalized diffusion equation for the time-dependent density field. This equation is similar to that found in dynamical DFT[30] such that it conserves the total density of the system. The continuous free energy function for the solid phase used in the common tangent construction was approximated by calculating free energies at discrete average densities and applying spline interpolation to obtain intermediate values.

The density profile at coexistence is computed under the constraint of constant average system density. The initial density field is found by setting up the aforementioned system box where the solid is constructed from the equilibrium solid density profile and the liquid is represented by a constant field with a density obtained from the common tangent construction. An example of the relaxed equilibrium DFT density profile (for $a' = 3.892$) is shown in Fig. 3.

TABLE VI. Melting temperature T_m', coexistence densities for the fluid, ρ_l', and the crystal, ρ_s', and $\Delta\rho'/\rho_s' = (\rho_s' - \rho_l')/\rho_s'$, as obtained from DFT and PFC (the densities ρ_l' and ρ_s' are given in units of ρ_s/κ^3).

a'	T_m'	ρ_l'	ρ_s'	$\Delta\rho'/\rho_s'$
DFT				
2.568	0.002062	0.06415	0.06442	0.004
3.892	0.000660	0.01923	0.01936	0.007
PFC				
2.568	0.002062	0.05395	0.05433	0.007
3.892	0.000660	0.01590	0.01610	0.012

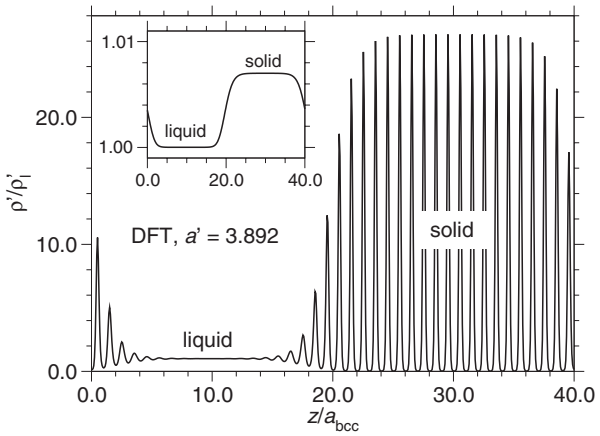

FIG. 3. Density profile in z direction (i.e., the direction perpendicular to the solid-liquid interface), as obtained in the framework of DFT. The density ρ is scaled by the liquid coexistence density ρ_l' while the distance z is in units of the linear dimension of a primitive bcc cell a_{bcc}. The inset shows the average density profile.

The interfacial free energy γ is obtained from the scaling relation

$$F(L_z) = f_{bulk} A L_z + \gamma A, \tag{25}$$

where $F(L_z)$ is the total free energy of the system, f_{bulk} is the bulk energy density, and A is the interfacial area. By changing the length of the system L_z, γ can be obtained from a linear fit. System boxes with $L_z = 30$, 32, 36, and 40 unit cells perpendicular to the liquid-solid interface were considered, and were found to give excellent linear scaling. This ensures also that there are no finite size effects due to the length of the box. Typically, $16 \times 16 \times 16$ grid points were used to resolve a unit bcc cell in the PFC while a higher resolution of $32 \times 32 \times 32$ grid points was necessary for the DFT calculations.

The results for different bcc surface orientations are shown in Table VII for the DFT and the PFC calculations.[58] First, we can conclude that the results from DFT are in reasonable agreement with the MD simulations for the (100) and (111) faces, and the dependence on a' is also weak. On the other hand, the PFC model gives interfacial free energies, which are about 2−3 times larger for both screening parameters. However, the most important difference between the MD and field theory calculations can be seen in the considerable relative anisotropies between the three high-symmetry facets given by the latter approaches. For example, for the screening parameter $a' = 2.568$ DFT and PFC predict relative asymmetries of about 30% between the (100) and (110) facets. These

TABLE VII. Dimensionless values for the interfacial energies ($\gamma\rho^{-2/3}/k_BT_m$) from the DFT and PFC calculations.

a'	γ_{100}	γ_{110}	γ_{111}
DFT			
2.568	0.150	0.104	0.167
3.892	0.142	0.098	0.157
PFC			
2.568	0.348	0.239	0.384
3.892	0.355	0.245	0.392

results are also in striking contrast with the case of interfacial free energy anisotropy bcc Fe, where PFC results are in good quantitative agreement with MD simulations.[33–35]

VI. SUMMARY AND CONCLUSIONS

In conclusion, we have presented data for the bcc crystal-fluid interfacial free energy for a Yukawa system.[23] In units of k_BT/a^2, the interfacial free energies at bcc crystal-fluid coexistence from MD simulations are much smaller than those at fcc crystal-fluid coexistence, which is in agreement with the Spaepen-Meyer theory. One of the implications is that the barrier of crystal nucleation is strongly reduced such that it would be easier to nucleate a bcc-crystal from the melt than a fcc-crystal.[55] Our results can in principle be verified by adjusting experimental data on crystal nucleation in charged suspensions[59–61] to classical nucleation theory, where the interfacial free energy enters as one of the crucial parameters.

Comparison between the results obtained from MD simulations and from DFT and PFC field theory approaches reveals interesting differences between the different methods. The magnitudes of the interfacial free energies between the MD data and DFT are in qualitative agreement, while the PFC model gives much larger values. The most striking difference, however, is that both field theory approaches predict a large anisotropy, up to more than 30% between the high-symmetry faces of bcc Yukawa systems.[23] This is somewhat surprising, since in the previously studied case of bcc Fe, the anisotropy was of the order of a few percent, as expected.[33–35] It would be interesting in the future to explicitly include noise (thermal fluctuations) in the DFT and PFC calculations to remedy the absence of capillary waves, which are important for large-scale thermal fluctuations of the interfaces.[62]

In principle, our method and analysis is directly transferable to other soft interactions (such as, e.g., Gaussian potentials), where we expect similar features for the interfacial free energy. For inverse power-law potentials, $u(r) \propto r^{-n}$ with $n = 6, 7, 8$, accurate estimates from MD simulations for the interfacial free energies of bcc-fluid interfaces have been reported in the work of Davidchack and Laird.[63] These estimates can be used as a testing bed for PFC and DFT calculations. Note that Davidchack and Laird[63] have also found that both the magnitude and anisotropy of the interfacial free energy is considerably smaller for bcc phases, relative to fcc phases of the same system. Another important generalization is toward dynamics where dynamical density functional theory can be used to extract the kinetic growth coefficients.[29] Finally, it would be interesting to generalize the method to liquid crystalline phases which are much more complex by, e.g., using related PFC models.[64,65]

ACKNOWLEDGMENTS

We thank Martin Oettel, Martin Grant, Ken Elder, and Mikko Karttunen for helpful discussions. This work was supported by the DFG within SPP 1296, and by the Academy of Finland through its Centres of Excellence Program (Project No. 251748).

[1] D. P. Woodruff, *The Solid-Liquid Interface* (Cambridge University Press, Cambridge/England, 1980).
[2] K. Binder and M. Müller, Int. J. Mod. Phys. C **11**, 1093 (2000).
[3] J. J. Hoyt, M. Asta, and A. Karma, Phys. Rev. Lett. **86**, 5530 (2001).
[4] R. L. Davidchack, J. R. Morris, and B. B. Laird, J. Chem. Phys. **125**, 094710 (2006).
[5] T. Zykova-Timan, R. E. Rozas, J. Horbach, and K. Binder, J. Phys.: Condens. Matter **21**, 464102 (2009).
[6] T. Zykova-Timan, J. Horbach, and K. Binder, J. Chem. Phys. **133**, 014705 (2010).
[7] R. E. Rozas and J. Horbach, Europhys. Lett. **93**, 26006 (2011).
[8] A. Härtel, M. Oettel, R. E. Rozas, S. U. Egelhaaf, J. Horbach, and H. Löwen, Phys. Rev. Lett. **108**, 226101 (2012).
[9] Y. Singh, Phys. Rep. **207**, 351 (1991).
[10] H. Löwen, Phys. Rep. **237**, 249 (1994).
[11] J. Z. Wu, AIChE J. **52**, 1169 (2006).
[12] J. F. Lutsko, Adv. Chem. Phys. **144**, 1 (2010).
[13] W. A. Curtin, Phys. Rev. Lett. **59**, 1228 (1987).
[14] W. A. Curtin, Phys. Rev. B **39**, 6775 (1989).
[15] R. Ohnesorge, H. Löwen, and H. Wagner, Phys. Rev. E **50**, 4801 (1994).
[16] D. W. Marr and A. P. Gast, Phys. Rev. E **47**, 1212 (1993).
[17] H. Löwen, T. Beier, and H. Wagner, Europhys. Lett. **9**, 791 (1989).
[18] R. Ohnesorge, H. Löwen, and H. Wagner, Phys. Rev. A **43**, 2870 (1991).
[19] C. N. Likos, Z. T. Németh, and H. Löwen, J. Phys.: Condens. Matter **6**, 10965 (1994).
[20] A. R. Denton and H. Löwen, Phys. Rev. Lett. **81**, 469 (1998).
[21] J.-L. Barrat, J.-P. Hansen, G. Pastore, and E. M. Waisman, J. Chem. Phys. **86**, 6360 (1987).
[22] See, e.g., A. Dekuiper, W. L. Vos, J. L. Barrat, J. P. Hansen, and J. A. Schouten, J. Chem. Phys. **93**, 5187 (1990).
[23] A. J. Archer, Phys. Rev. E **72**, 051501 (2005).
[24] T. V. Ramakrishnan and M. Yussouff, Phys. Rev. B **19**, 2775 (1979).
[25] M. Renkin and J. Hafner, J. Chem. Phys. **94**, 541 (1991).
[26] D. C. Wang and A. P. Gast, J. Chem. Phys. **112**, 2826 (2000).
[27] D. C. Wang, and A. P. Gast, J. Phys.: Condens. Matter **11**, 10133 (1999).
[28] K. R. Elder, N. Provatas, J. Berry, P. Stefanovic, and M. Grant, Phys. Rev. B **75**, 064107 (2007).
[29] S. van Teeffelen, H. Löwen, R. Backofen, and A. Voigt, Phys. Rev. E **79**, 051404 (2009).
[30] H. Emmerich, H. Löwen, R. Wittkowski, T. Gruhn, G. I. Tóth, G. Tegze, and L. Gránásy, Adv. Phys. **61**, 665 (2012).
[31] K. R. Elder, M. Katakowski, M. Haataja, and M. Grant, Phys. Rev. Lett. **88**, 245701 (2002).
[32] K. R. Elder and M. Grant, Phys. Rev. E **70**, 051605 (2004).
[33] D. Y. Sun, M. Asta, J. J. Hoyt, M. I. Mendelev, and D. J. Srolovitz, Phys. Rev. B **69**, 020102(R) (2004).
[34] A. Jaatinen, C. V. Achim, K. R. Elder, and T. Ala-Nissila, Phys. Rev. E **80**, 031602 (2009).
[35] A. Jaatinen, C. V. Achim, K. R. Elder, and T. Ala-Nissila, Tech. Mech. **30**, 169 (2010).
[36] H. Löwen and G. Kramposthuber, Europhys. Lett. **23**, 683 (1993).
[37] H. Löwen and E. Allahyarov, J. Phys.: Condens. Matter **10**, 4147 (1998).
[38] C. P. Royall, M. E. Leunissen, A.-P. Hynninen, M. Dijkstra, and A. van Blaaderen, J. Chem. Phys. **124**, 244706 (2006).
[39] G. E. Morfill and A. V. Ivlev, Rev. Mod. Phys. **81**, 1353 (2009).
[40] A. V. Ivlev, H. Löwen, G. E. Morfill, and C. P. Royall, *Complex Plasmas and Colloidal Dispersions: Particle-Resolved Studies of Classical Liquids and Solids* (World Scientific, Singapore, 2012).
[41] S. A. Khrapak, B. A. Klumov, P. Huber, V. I. Molotkov, A. M. Lipaev, V. N. Naumkin, H. M. Thomas, A. V. Ivlev, G. E. Morfill, O. F. Petrov, V. E. Fortov, Y. Malentschenko, and S. Volkov, Phys. Rev. Lett. **106**, 205001 (2011).
[42] M. O. Robbins, K. Kremer, and G. S. Grest, J. Chem. Phys. **88**, 3286 (1988).
[43] E. J. Meijer and D. Frenkel, J. Chem. Phys. **94**, 2269 (1991).
[44] S. Hamaguchi, R. T. Farouki, and D. H. Dubin, Phys. Rev. E **56**, 4671 (1997).
[45] O. S. Vaulina, S. A. Khrapak, and G. E. Morfill, Phys. Rev. E **66**, 016404 (2002).
[46] A. Mijailovic, R. E. Rozas, J. Horbach, and H. Löwen, "Liquid-solid interfacial free energy of fcc Yukawa systems" (unpublished).
[47] F. Spaepen, Acta Metall. **23**, 729 (1975).
[48] F. Spaepen and R. B. Meyer, Scr. Metall. **10**, 257 (1976).
[49] A. Alexander and J. McTague, Phys. Rev. Lett. **41**, 702 (1978).

[50]H. C. Andersen, J. Chem. Phys. **72**, 2384 (1980).
[51]M. D. Carbajal-Tinoco, J. Chem. Phys. **128**, 184507 (2008).
[52]A. Jaatinen and T. Ala-Nissila, Phys. Rev. E **82**, 061602 (2010).
[53]M. Oettel, S. Dorosz, M. Berghoff, B. Nestler, and T. Schilling, Phys. Rev. E **86**, 021404 (2012).
[54]P. J. Steinhardt, D. R. Nelson, and M. Ronchetti, Phys. Rev. B **28**, 784 (1983).
[55]P. R. Ten Wolde, M. J. Ruiz-Montero, and D. Frenkel, Phys. Rev. Lett. **75**, 2714 (1995).
[56]Note that only the low-q data (up to $q = 0.47$) is taken into account for the extrapolation towards $q \to 0$. Very similar results for $\bar{\gamma}$ are obtained using the naked eye to read off the constant value in $\bar{\gamma}(q)$ at small values of q.
[57]W. R. Fehlner and S. H. Vosko, Can. J. Phys. **54**, 2160 (1976).
[58]We note that because of technical reasons, the values of the screening parameters are slightly different between the MD simulations and the field theory approaches. However, due to the weak dependence of the interfacial free energies on a' the results are directly comparable between $a' = 2.50$ and 2.57, and $a' = 4.0$ and 3.89, respectively.
[59]P. Wette, H.-J. Schöpe, and T. Palberg, J. Chem. Phys. **123**, 174902 (2005).
[60]D. M. Herlach, I. Klaasen, P. Wette, and D. Holland-Moritz, J. Phys.: Condens. Matter **22**, 153101 (2010).
[61]T. Palberg, J. Phys.: Condens. Matter **11**, R323 (1999).
[62]J. D. Weeks, J. Chem. Phys. **67**, 3106 (1977).
[63]R. L. Davidchack and B. B. Laird, Phys. Rev. Lett. **94**, 086102 (2005).
[64]H. Löwen, J. Phys.: Condens. Matter **22**, 364105 (2010).
[65]C. V. Achim, R. Wittkowski, and H. Löwen, Phys. Rev. E **83**, 061712 (2011).